Journal of X-Ray Science and Technology 16 (2008) 189–201
IOS Press

Retinal vessel enhancement and extraction based on directional field

Jian Chen[a], Jie Tian[a,b,*], Zichun Tang[a], Jian Xue[a], Yakang Dai[a] and Jian Zheng[a]
[a]*Institute of Automation, Chinese Academy of Sciences, Beijing, 100190, P.R. China*
[b]*Life Science Center, Xidian University, Xian, Shanxi, 710071, P.R. China*

Received 18 December 2007
Revised 19 May 2008
Accepted 20 June 2008

Abstract. In order to extract the low contrast vessels in retinal images, we propose a novel enhancement algorithm based on directional field and develop a robust retinal vessel extraction framework. The proposed enhancement algorithm can significantly improve the contrast of vasculature especially the slim vessels and low contrast vessels. In our framework, we first enhance the vasculature by the proposed enhancement algorithm, and extract the vessels from the enhanced image by a local extraction method. Secondly, we apply a series of modified top-hat transform to original image, and use a binary morphological reconstruction to extract the large size vessels. Finally, the whole vasculature is provided by an organic combination algorithm. The first step extracts the slim vessels and low contrast vessels well but misses some bifurcations and cross pixels. On the other hand, the second step preserves the bifurcations and cross pixels but misses some slim vessels and low contrast vessels. Therefore, the combination of the two methods can provide satisfactory extraction of vasculature. Experimental results show that our method outperforms existing algorithms in terms of sensitivity and accuracy when testing on 'DRIVE' and 'STARE' databases.

1. Introduction

In ophthalmic practice, optic fundus photography technique has become a common procedure to diagnose lots of retinopathies. The retina is the unique region of the human body where the vascular condition can be directly observed in vivo. The extraction of vasculature in retina images plays an important role when diagnosing and treating some ophthalmic diseases like choroidal neovascularization [4], retinal artery occlusion [23], and glaucoma. Moreover, many world-wide non-ophthalmic diseases, such as diabetes mellitus, hypertension, arteriosclerosis, cardiovascular disease [9], and stroke also reveal the retinal pathological changes.

A lot of vessel extraction algorithms have been developed recently. All these algorithms can be generally grouped as *supervised methods* and *rule-based methods*. The former group requires manually labeled images to train the classifier [13,17]. These methods are promising because of their good performance. However, the manual assessment are usually tedious, time-consuming, error-prone or even impossible when encountering some extreme cases. The latter group, *rule-based methods*, assesses the

*Corresponding author. Jie Tian, Institute of Automation, Chinese Academy of Sciences, Zhongguancun East Rd. 95, Haidian Dist., Beijing, 100190, P.R. China. Tel.: +86 10 82628760; Fax: +86 10 62527995; E-mail: tian@ieee.org.

retinal images by some rules designed in advance. These methods can be subdivided into *tracking-based methods* and *pixel processing-based methods*. *Tracking-based methods* [5,7,10,18] start from vessel seeds which are manually or semi-automatically located, and trace the vessels along with vessel direction under some specific rules, and finally stop when the tracing pixel breaks the rules. *Pixel processing-based methods* are very popular in recent years [6,11,12,15,16,19–22]. One common ground of such methods is that they process the image pixel by pixel. They will collect the local information of neighborhood of the pixel and judge whether the current pixel belongs to the vessel or not. Matched filter [16], dynamic thresholding, model-based algorithms [19] and mathematical morphology algorithms are all such methods.

Aforementioned algorithms cannot extract the vessels properly when the vascular contrast is lower than a critical threshold. In fundus image, the capillary vessels of retina generally have low contrast. Moreover, the vessels affected by some retinopathies are also of low contrast.

This paper proposed a low contrast vessel enhancement and extraction algorithm based on directional field (DF). To the best of our knowledge, there was no literature about vascular enhancement and extraction using precise DF. Actually, the retinal vessels have the property that its orientation and gray intensity vary slowly along the vessels. This property makes it possible to obtain precise DF of retinal image and then enhance the vasculature. In this paper, we get the enhancement done along the vascular direction, and highlight the vasculature by the directional Gabor filter. We also present a framework to extract the whole vasculature, and quantitatively compare our method with other algorithms.

2. Methods

In this section, we first introduce the proposed enhancement algorithm, and then we will present the framework of retinal vessel extraction.

2.1. Enhancement

2.1.1. Estimation of DF

An accurate DF is needed to enhance the image contrast in our method. Here we introduce a continuous method named *averaging squared gradients* [3,8]. In the following text, three parameters of DF, the direction θ, the coherence coh and the strength str, are estimated.

For each image sample, $I(x, y)$, the gradient vector $[G_x(x, y)\ G_y(x, y)]^T$ is defined as follows:

$$\begin{bmatrix} G_x(x,y) \\ G_y(x,y) \end{bmatrix} = \text{sign}\left(\frac{\partial I(x,y)}{\partial x}\right) \begin{bmatrix} \frac{\partial I(x,y)}{\partial x} \\ \frac{\partial I(x,y)}{\partial y} \end{bmatrix},$$

The second element of the gradient vector has been chosen to always be positive. The reason for this choice is that opposite directions of gradient indicate equivalent orientations in DF. Gradients cannot be averaged directly since opposite gradient vectors will then cancel each other, although they indicate the same orientation. A solution to this problem is proposed by squaring the gradient vector considered as a complex number before averaging. With this solution, the angle of gradient vector is doubled and the length is squared, therefore, the opposite gradient vectors will point to the same direction. For doubling the angle and squaring the length, the gradient vector is converted to polar coordinates:

$$\begin{bmatrix} G_\rho \\ G_\varphi \end{bmatrix} = \begin{bmatrix} \sqrt{G_x^2 + G_y^2} \\ \tan^{-1}(G_y/G_x) \end{bmatrix},$$

then the squared gradient vectors $[G_{s,x}\ G_{s,y}]^T$ is given by:

$$\begin{bmatrix} G_{s,x} \\ G_{s,y} \end{bmatrix} = \begin{bmatrix} G_\rho^2 \cos(2G_\varphi) \\ G_\rho^2 \sin(2G_\varphi) \end{bmatrix} = \begin{bmatrix} G_x^2 - G_y^2 \\ 2G_x G_y \end{bmatrix}.$$

Next, the average squared gradient $[\overline{G_{s,x}}\ \overline{G_{s,y}}]^T$ can be calculated as follows:

$$\begin{bmatrix} \overline{G_{s,x}} \\ \overline{G_{s,y}} \end{bmatrix} = \begin{bmatrix} \sum_W G_{s,x} \\ \sum_W G_{s,y} \end{bmatrix}$$

where W is the window of averaging filter. This operation will reinforce each other when gradient vectors are opposite.

The gradient vectors have to be converted back to their single angle representation. Now, the average gradient direction Φ, with $-\frac{1}{2}\pi < \Phi < \frac{1}{2}\pi$, is given by:

$$\Phi = \frac{1}{2}\angle(\overline{G_{s,x}}, \overline{G_{s,y}})$$

$$\angle(x,y) = \begin{cases} \tan^{-1}(y/x) & x \geqslant 0 \\ \tan^{-1}(y/x) + \pi & x < 0\ \&\ y \geqslant 0 \\ \tan^{-1}(y/x) - \pi & x < 0\ \&\ y < 0 \end{cases}$$

and the average direction θ of DF, with $-\frac{1}{2}\pi < \theta < \frac{1}{2}\pi$, is perpendicular to Φ:

$$\theta = \begin{cases} \Phi + \frac{1}{2}\pi & \Phi \leqslant 0 \\ \Phi - \frac{1}{2}\pi & \Phi > 0 \end{cases}$$

The coherence coh indicates how well all squared gradients in a local neighborhood share the same orientation. It is defined as:

$$coh = \frac{|\sum_W (G_{s,x}, G_{s,y})|}{\sum_W |(G_{s,x}, G_{s,y})|}$$

The strength str indicates the sum of the moduli of the gradient vectors in a local neighborhood. It is defined as:

$$str = \frac{\sum_W G_\rho}{\max(\sum_W G_\rho)}$$

The sizes of windows are 9×9 to the direction but 5×5 to the coherence and the strength. We do not use the same size of window because the mean value of directions in a bigger window is much more accurate than that in a smaller window. But the coherence and the strength are barely affected by the size of window. The example of DF is shown in Fig. 1.

2.1.2. Enhancement based on DF

The principal objective of enhancement is to process an image so the resulting image has increased contrast. In this subsection, we propose a novel method to enhance the retinal image.

Assume $M(x,y)$ and $V(x,y)$ are the estimated mean and variance value at image sample $I(x,y)$. It is obvious that $V(x,y)$ is small if there is no vessel in this neighborhood. Thus we employed a threshold

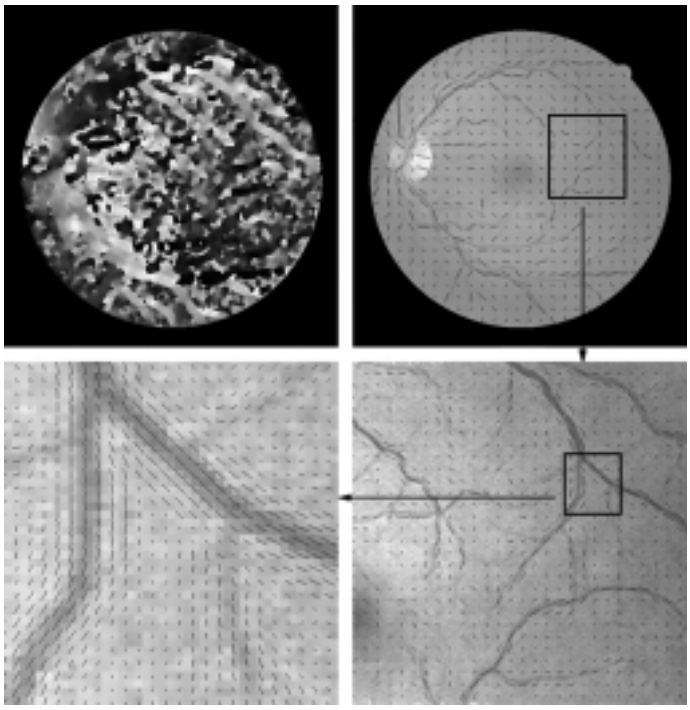

Fig. 1. Directional field. Top left: Gray-scale coded DF. The others: Line-matrix representation of DF.

of variance to distinguish the non-vessel areas and vessel areas. In order to enhance the low contrast vessel, the threshold is set to a very small value.

For each image sample, $I(x, y)$, the local normalization is defined as follows:

$$T(i,j,x,y) = \begin{cases} M_0 + f(V(i,j))\sqrt{I(x,y) - M(i,j)} & \text{if } I(x,y) > M(i,j) \\ M_0 - f(V(i,j))\sqrt{I(x,y) - M(i,j)} & \text{otherwise} \end{cases}$$

where M_0 is the desired mean value, $f(V(i,j))$ is the weighting function of variance, $T(i,j,x,y)$ denotes the weighted normalization for pixel (x,y) when the center of normalization is at pixel (i,j).

To get the enhanced image, we calculate the total sum of weighted normalization at a local neighborhood:

$$I_E(x,y) = I(x,y) + \sum_{(i,j)\in W} (T(i,j,x,y) - I(x,y))g(x-i, y-j)$$

where g denotes the 2D Gaussian kernel and $\sum_W g = 1$. The main purpose of Gaussian kernel is to reduce the weight when the center of normalization is far away to the pixel (x,y), which ensures the good performance of enhancement and eliminates the artificial boundary of local normalization.

The aforementioned weighting function by variance is defined as follows:

$$f(V(i,j)) = \begin{cases} c_h & \text{if } V_{ij} > V_{TH} \\ c_l & \text{if } V_{ij} < V_{TL} \\ c_0 \cdot {V_{ij}}^{c_1} & \text{otherelse} \end{cases}$$

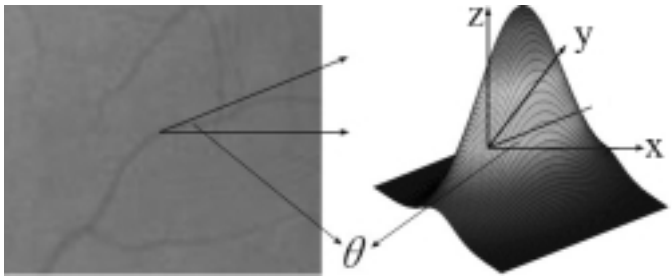

Fig. 2. Left: A segment of retinal image. Right: Surface representation of anisotropic Gaussian kernel.

where V_{TH}, V_{TL} are two thresholds of variance and $V_{TH} > V_{TL}$, c_h is a comparatively large constant while c_l is small one. The purpose of this weighting function is to tune the degree of enhancement. If the variance is greater than the high threshold V_{TH}, we will limit its enhancement. On the other hand, if the variance is lower than V_{TL}, this local area will be smoothed because there is no vessel. Between these two situations, c_0 and c_1 are used to control the weighting function, thus providing the required enhancement.

In order to obtain better results, we apply anisotropic Gaussian kernel instead of isotropic kernel. The orientation of Anisotropic Gaussian kernel is completely determined by the local vascular orientation as shown in Fig. 2.

The sizes of windows used in this subsection are all 9×9 pixels.

2.1.3. Directional filtering by Gabor filter

The configurations of two parallel edges of a vessel with well-defined orientation in a retinal image provide useful information which helps in removing undesired noise and preserving the true vessels. In this paper, we apply even-symmetric Gabor filter to remove the noise:

$$h_{\mathsf{e}}(x, y, \theta, a) = \exp\left[-\frac{1}{2}\left(\frac{x_\theta^2}{\sigma_x^2} + \frac{y_\theta^2}{\sigma_y^2}\right)\right] \cdot \cos(a x_\theta)$$

$$x_\theta = x\cos\theta + y\sin\theta$$

$$y_\theta = -x\sin\theta + y\cos\theta$$

where θ denotes the direction of Gabor filter, a is the frequency of complex exponential, σ_x and σ_y are the standard deviations of the Gaussian envelope along x and y axes respectively. The selection of the values of σ_x and σ_y involves a trade-off. The larger the values, the more robust to noise the filters are but the more likely the filters will create spurious vessels. On the other hand, the smaller the values, the less likely the filters will create spurious vessels; consequently they will be less effective in removing the noise. In this paper, the values of both σ_x and σ_y are set to 4.0 based on empirical data. The direction θ is exactly the same as the direction of DF. The frequency a is determined by the width of vessels. To detect the vessels with various widths, a is assigned to 2 and 4 respectively. The results of Gabor filtering with different frequencies are shown in Fig. 3.

Let I be the enhanced image, I_θ be the directions, the filtered image I_f is obtained as follows:

$$I_f(x, y) = \sum_{(u,v)\in W} h_{\mathsf{e}}(u, v, I_\theta(x, y), a) I(x - u, y - v).$$

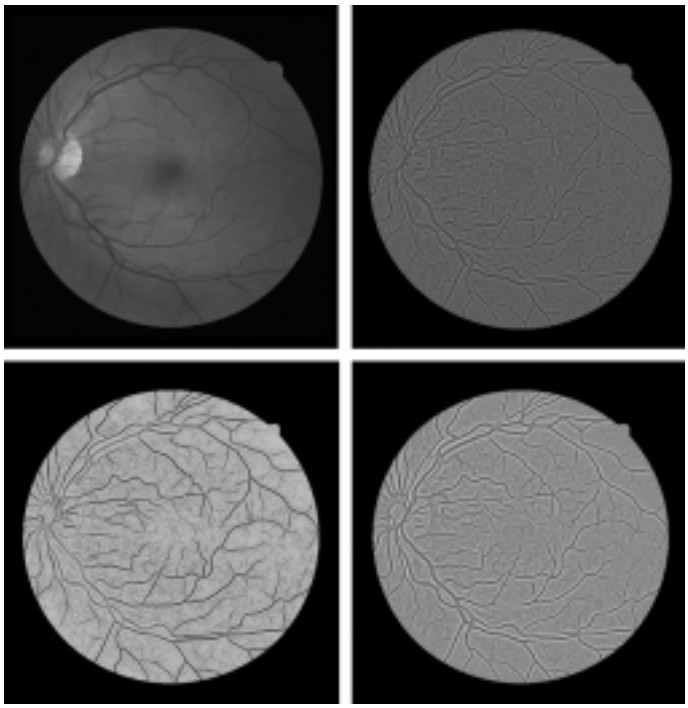

Fig. 3. Results of enhancement and Gabor filtering. Top left: Original image. Top right: Enhanced image. Bottom: Results of Gabor filter with different frequency a = 2 and 4.

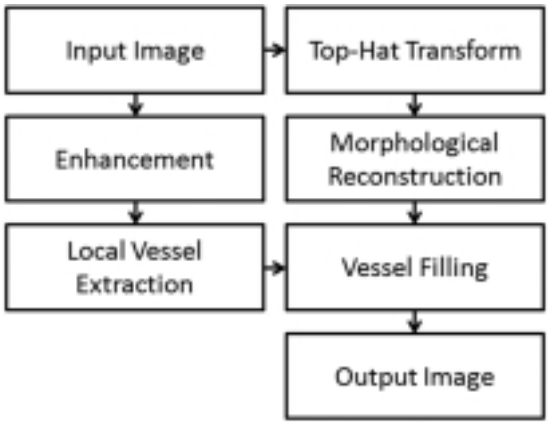

Fig. 4. The flowchart of the proposed vessel extraction algorithm.

2.2. Retinal vessel extraction framework

We present our retinal vessel extraction framework in this subsection. In our framework, we first extract the vessels from the enhanced image by a local extraction method. Secondly, we apply a series of modified top-hat transform to original image, and use a binary morphological reconstruction to extract the large size vessels. Finally, the whole vasculature is provided by an organic combination algorithm. The flowchart of the proposed extraction technique is shown in Fig.4.

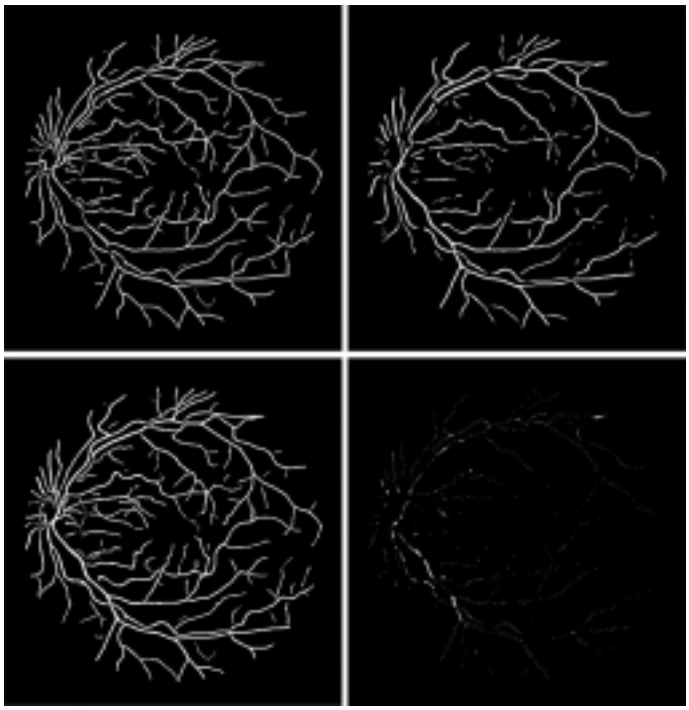

Fig. 5. Local vessel extraction. Top: Results of local vessel extraction on enhanced images with a $= 2$ and a $= 4$ respectively. Bottom left: The final output of local vessel extraction. Bottom right: subtraction of the image on top left from the image on bottom left. It can be seen that the vessels are more integrated in the final output of local vessel extraction.

2.2.1. Local vessel extraction from enhanced image

We develop a local vessel extraction algorithm to extract the vasculature from enhanced images. At each pixel, the mean values in a circle neighborhood and in an ellipse neighborhood along the vessel direction are estimated. The current pixel is classified to vasculature or background according to the comparison of the two mean values. To facilitate the implement, we use a 11×11 rectangular neighborhood to represent the circle neighborhood and use a 3×11 rectangular neighborhood to represent the ellipse neighborhood. Assume the mean values of circle neighborhood and ellipse neighborhood are M_c and M_e respectively. The decision rule is as follows:

$$p(x,y) \in \begin{cases} V \text{ if } \ M_c(x,y) - M_e(x,y) > \epsilon \\ B \text{ otherwise} \end{cases}$$

where V stands for vasculature, B for background, ϵ is a small positive number.

There are lots of noises in the binary vascular image provided by local vessel extraction algorithm. Fortunately, the connected components of these noises are generally smaller than the vessel's. We apply a connected component detection algorithm to remove those noises and keep the vasculature. The original image and local vessel extraction are shown in Fig. 5.

2.2.2. Top-hat transform and morphological reconstruction

This step is for extracting the main structures of retinal image, and it is applied on original image for the reason that Some bifurcations are filtered out by Gabor filter in enhanced image.

The classical top-hat operator which calculated by subtracting the opened image from the original image is sensitive to noise. In our framework, a sequence of modified top-hat operators [12] with circular structuring elements of increasing radius have been employed to remove the background,

$$\mathrm{TH}_I = I - \min((I \bullet S_c) \circ S_o; I)$$

where $(\bullet)$ and $(\circ)$ denotes the closing and opening operations of gray-scale images respectively. S_c is the structuring element of closing and has a fixed size of 1 pixel. $S_\circ$ is structuring element of opening and have the increasing size from 1 to 8 pixels. Eight images at various scales are yielded and finally reduced to four; each one obtained as the average of two responses of operators with consecutive radius.

The four images resulting from the modified top-hat operators are used for reconstructing potential vessels. Reconstruction is a morphological transformation involving two images. One image, the *marker*, is the starting point for the transformation. The other image, the *mask*, constrains the transformation. Two thresholds, τ_l and τ_h, are used to get the mask and marker images by thresholding operation. The results of morphological reconstruction are shown in Fig. 6.

2.2.3. Vessel filling

The first step in our framework provide the slim vessels and low contrast vessels, and the second step provide the main structures. Now we develop a vessel filling algorithm to get the final vasculature.

Assume the results of the first and second steps are I_τ and I_R respectively. A pixel is classified to vasculature if it meet one of the following three rules:

1. $I_\tau \cap I_R$
2. $I_\tau \cap (\neg I_R) \cap (coh \geqslant coh_\tau)$
3. $I_R \cap (\neg I_\tau) \cap (str \geqslant str_\tau)$

where coh_τ and str_τ are thresholds of coh and str respectively. The first step extracts the slim vessels and low contrast vessels well but misses some bifurcations and cross pixels. On the other hand, the second step preserves the bifurcations and cross pixels but misses some slim vessels and low contrast vessels. Therefore, the combination of the two methods can provide satisfactory extraction of vasculature. The final vessel extraction is obtained by a filling operation aiming at removing all pixels completely surrounded by vessel points, but not labeled as vessel. We get this job done by the criterion that a pixel with more than six neighbors classified as vessel must also be labeled as vessel.

3. Results

3.1. Data and evaluation

Two publicly available databases, 'DRIVE' [2,14] and 'STARE' [1], are used to test the proposed algorithm. Both databases have manual segmentations which can be used as ground truth. A lot of retinal vascular extraction algorithms have been tested on the two databases; therefore a quantitative comparison can be easily implemented between our method and the others. The green channel of original RGB color image has been chosen to evaluate the proposed algorithm.

The DRIVE database were collected by Staal and consisted of 40 images (7 pathological images). It was divided into a train set with 20 images (3 pathological images) and a test set with another 20 images (4 pathological images). These images were originally captured from a Canon CR5 nonmydriatic 3 CCD

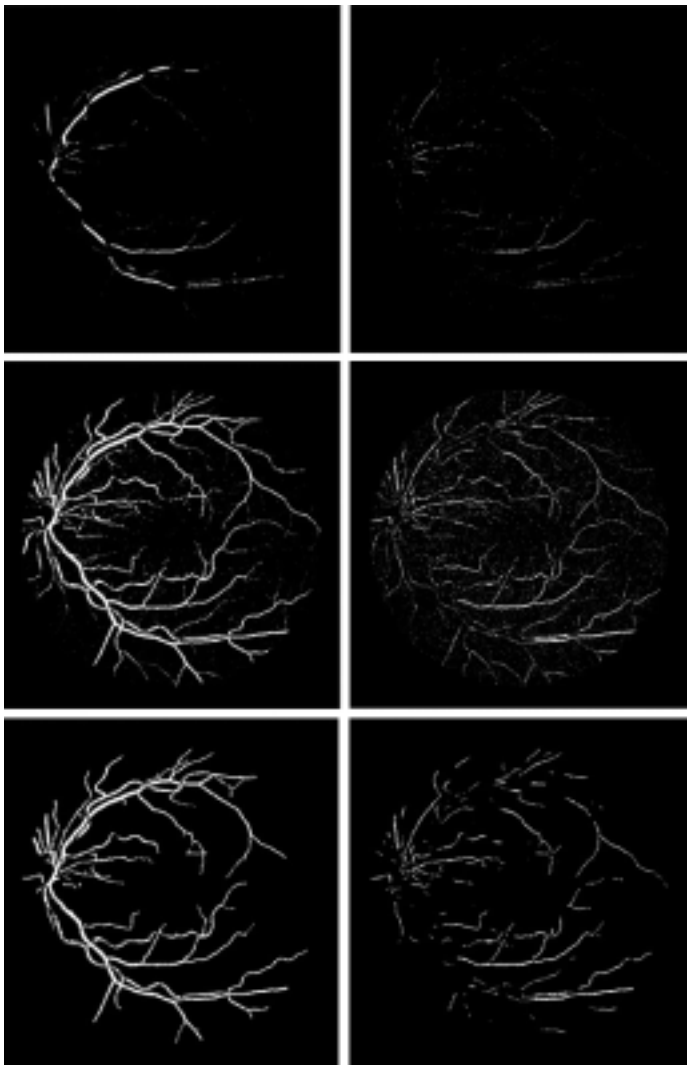

Fig. 6. Results of the morphological reconstruction. Top row: Marker image. Middle row: Mask image. Bottom row: Output of the morphological reconstruction operator.

camera at 45° field of view, with the size of 565×584 pixels, 8 bits per color channel and have a field of view (FOV) of approximately 540 pixels in diameter. Our experiments were all masked by FOV. The images in the test set were manually segmented twice by two observers, resulting in set A and set B. The observer of set A marked 577,649 pixels as vessel and 3,960,494 pixels as background (12.7% vessel), and the number for set B are 556,532 pixels as vessel and 3,981,611 pixels as background (12.3% vessel) respectively. The set A are used as ground truth.

The STARE database were collected by Hoover and consisted of 20 images (10 pathological images). These images were originally captured from a TopCon TRV 50 camera at 35° field of view, with the size of 700×605 pixels, 8 bits per color channel and have a FOV of approximately 650×550 pixels in diameters. Two observers segmented these images. The first observer marked 615,726 pixels as vessel and 5,293,034 pixels as background (10.4% vessel), and the number for the second observer are 879,695

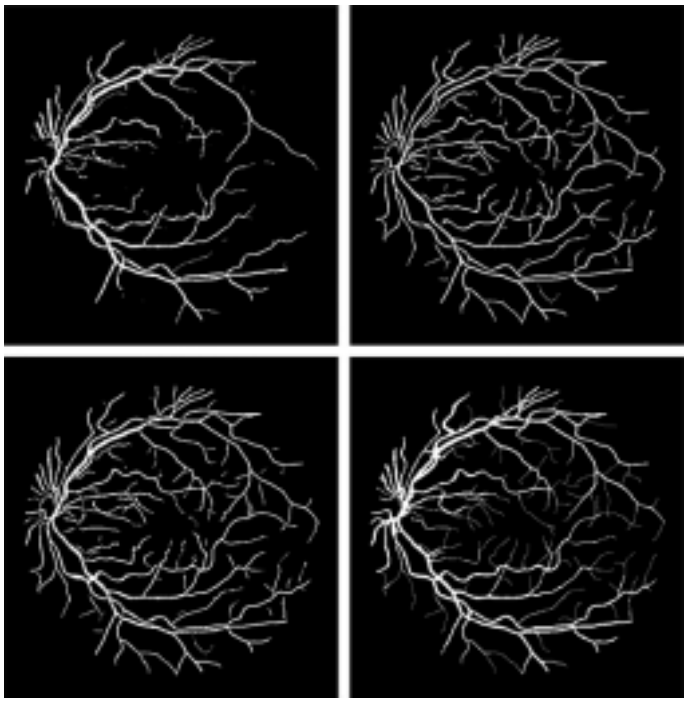

Fig. 7. Normal case of DRIVE database. Top: Intermediate results. Bottom left: Final result of the proposed method. Bottom right: Ground truth.

pixels as vessel and 5,029,065 pixels as background (14.9% vessel) respectively. The segmentations by the first observer were used as ground truth. The significant difference between the observers suggests the hardness of vascular extraction on this database.

Three statistical measures, sensitivity (SE), specificity (SP) and accuracy (AC) have been estimated for each test image. The sensitivity is estimated by the ratio of the number of correctly classified vascular pixels by the number of pixels of vessel in ground truth. The specificity is estimated by the ratio of the number of correctly classified background pixels by the number of pixels of background in ground truth. The accuracy is by the ratio of total number of correctly classified pixels by the number of pixels in the image field of view.

3.2. Experimental results

Figures 7 and 8 show two cases of vessel extraction by our method. In which the intermediate results, the final results and the ground truth are displayed. The original image of the first case is chosen from 'DRIVE' database and is shown on top left of Fig. 3. The second case is chosen from 'STARE' database and is affected by retinopathy.

Comparative results are shown in Table 1. The manual segmentations from the second observer, the segmentations of our method, and the segmentations of the methods reported by Staal [17], Mendonca [12] and Li Wang [21] are compared. Table 1 presents the average sensitivity, specificity and accuracy on both databases. Some values are unavailable in literatures, so this table is not integrated. The comparative results show a great improvement of our method on sensitivity because of the enhancement of low contrast vessels.

Table 1
Performance of vessel segmentation methods

	Method	SE/SD*	SP/SD	AC/SD
STARE	2nd observer	0.8951/ 0.1085	0.9385/ 0.0260	0.9350/ 0.0168
	Staal [17]	0.6898/ 0.1558	0.9793/ 0.0133	0.9516/ –
	Li Wang [21]	0.7543/ 0.0596	0.9785/ 0.0106	–
	Mendonca [12]	0.7123/ –	0.9758/ –	0.9479/ 0.0123
	Our Method	0.7737/ 0.0735	0.9738/ 0.0169	0.9490/ 0.0109
DRIVE	Set B	0.7760/ 0.0594	0.9725/ 0.0083	0.9473/ 0.0048
	Staal [17]	0.7194/ 0.0694	0.9773/ 0.0087	0.9441/ 0.0065
	Li Wang [21]	0.7810/ 0.0340	0.9770/ 0.0071	–
	Mendonca [12]	0.7315/ –	0.9781/ –	0.9463/ 0.0065
	Our Method	0.7583/ 0.0449	0.9778/ 0.0064	0.9462/ 0.0057

*The acronym for the standard deviation.
– Not available.

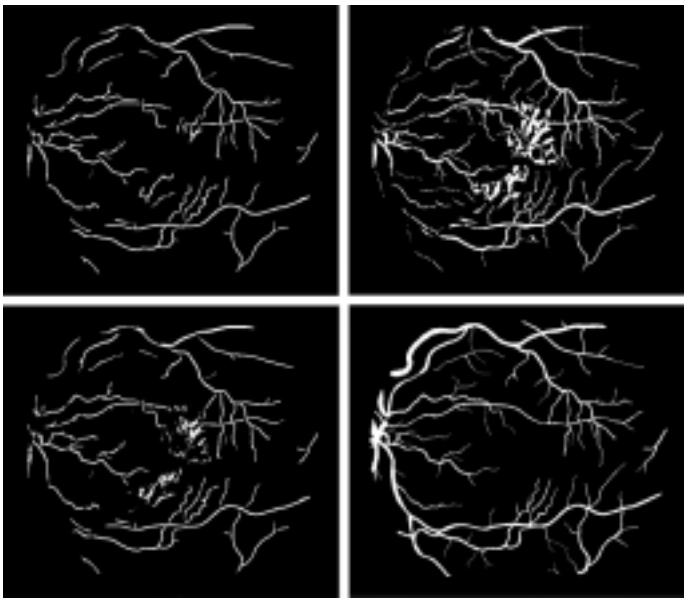

Fig. 8. Abnormal case of STARE database. Top: Intermediate results. Bottom left: Final result of the proposed method. Bottom right: Ground truth.

4. Discussion and conclusion

The false extractions of existing algorithms, such as [12,15], are mainly derived from the slim vessels and low contrast vessels. The proposed algorithm which aims at resolving these problems improves the extraction significantly.

The main contribution of this paper is the image enhancement algorithm. Lots of slim vessels and low contrast vessels are displayed clearly after enhancement. This can be seen from Fig. 3. However, the enhancement technique also bring some noise when the weighting function (see section II) is inappropriate. Fortunately, the most of the noise can be eliminated by Gabor filter.

The maximum response of Gabor filter is reached when the Gabor filter and the vessel have exactly the same direction. Soares [15] applied Gabor filter with 18 directions on retinal image independently

to highlight the directional vessels. In this paper, we assign the direction of Gabor filter to the direction of DF at each pixel. This means the direction of Gabor filter in our method is always the same as the direction of vessel. Theoretically, our Gabor filter is 18 times faster than Soares's. Our Gabor filter has another advantage that the computational complexity will not increase when increasing the directional resolution. Comparatively, the computational complexity of Soares's algorithm will increase linearly when increasing directions.

The proposed enhancement algorithm can be applied to enhance other images. For example, we can enhance the cardiac CT image with the proposed algorithm. In our future work, we will mainly concentrate on applying the proposed algorithm on other image enhancement fields.

Acknowledgment

This paper is supported by the Project for the National Basic Research Program of China (973) under Grant No. 2006CB705700, 863 program under Grant No. 2006AA04Z216, the Joint Research Fund for Overseas Chinese Young Scholars under Grant No. 30528027, Changjiang Scholars and Innovative Research Team in University (PCSIRT) under Grant No. IRT0645, CAS Hundred Talents Program, CAS Scientific Research Equipment Development Program (YZ0642, YZ200766), the National Natural Science Foundation of China under Grant No. 30600151, 30672690, 60621001, 30500131, 60532050, Beijing Natural Science Fund under Grant No. 4071003.

References

[1] http://www.ces.clemson.edu/ ahoover/stare.
[2] http://www.isi.uu.nl/Reseach/Databases/DRIVE/results.php.
[3] A.M. Bazen and S.H. Gerez, Systematic methods for the computation of the directional fields and singular points of fingerprints, *IEEE Trans Pattern Anal Mach Intell* **24**(7) (July 2002), 905–919.
[4] D.E. Becker, A. Can, J.N. Turner, H.L. Tanenbaum and B. Roysam, Image processing algorithms for retinal montage, synthesis, mapping and realtime location determination, *IEEE Trans Biomed Eng* **45**(1) (Jan 1998), 115–118.
[5] A. Can, H. Shen, J.N. Turner, H.L. Tanenbaum and B. Roysam. Rapid automated tracing and feature extraction from retinal fundus images using direct exploratory algorithms, *IEEE Trans Inf Technol Biomed* **3**(2) (June 1999), 125–138.
[6] L. Gang, O. Chutatape and S.M. Krishnan, Detection and measurement of retinal vessels in fundus images using amplitude modified second-order gaussian filter, *IEEE Trans Biomed Eng* **49**(2) (Feb. 2002), 168–172.
[7] E. Grisan, A. Pesce, A. Giani, M. Foracchia and A. Ruggeri, A new tracking system for the robust extraction of retinal vessel structure. In *Proceedings of the 26th Annual International Conference of the IEEE EMBS*, San Francisco, CA, USA, September 1–5, 2004.
[8] L. Hong, Y. Wan and A. Jain, Fingerprint image enhancement: Algorithm and performance evaluation, *IEEE Trans Pattern Anal Mach Intell* **20**(8) (Aug. 1998), 777–789.
[9] J.J. Kanski, *Clinical Ophthalmology: A Systematic Approach*, London, U.K.: Butterworth-Heinemann, 1989.
[10] M. Lalondey, L. Gagnony and M.-C. Boucher, Non-recursive paired tracking for vessel extraction from retinal images. In Presented at the Conference Vision Interface, Montreal, 2000.
[11] J. Lowell, A. Hunter, D. Steel, A. Basu, R. Ryder and R.L. Kennedy, Measurement of retinal vessel widths from fundus images based on 2-d modeling, *IEEE Trans Med Imag* **23**(10) (Oct. 2004), 1196–1204.
[12] A.M. Mendonca and A. Campilho, Segmentation of retinal blood vessels by combining the detection of centerlines and morphological reconstruction, *IEEE Trans Med Imag* **25**(9) (Sep. 2006), 1200–1213.
[13] R. Nekovei and Y. Sun, Back-propagation network and its configuration for blood vessel detection in angiograms, *IEEE Trans Neural Netw* **6**(1) (Jan. 1995), 64–72.
[14] M. Niemeijer, J. Staal, B. van Ginneken, M. Loog and M.D. Abramoff, Comparative study of retinal vessel segmentation methods on a new publicly available database, in: *Proc. SPIE Med. Imag.*, M. Fitzpatrick and M. Sonka, eds, 5370:648–656, 2004.
[15] J.V.B. Soares, J.J.G. Leandro, R.M. Cesar Jr., H.F. Jelinek and M.J. Cree, Retinal vessel segmentation using the 2-d gabor wavelet and supervised classification, *IEEE Trans Med Imag* **25**(9) (Sep. 2006), 1214–1222.

[16] M. Sofka and C.V. Stewart, Retinal vessel centerline extraction using multiscale matched filters, confidence and edge measures, *IEEE Trans Med Imag* **25**(12) (Dec. 2006), 1531–1546.
[17] J. Staal, M.D. Abramoff, M. Niemeijer, M.A. Viergever and B. van Ginneken, Ridge-based vessel segmentation in color images of the retina, *IEEE Trans Med Imag* **23**(4) (April 2004), 501–509.
[18] Y. Tolias and S.M. Panas, A fuzzy vessel tracking algorithm for retinal images based on fuzzy clustering, *IEEE Trans Med Imag* **17**(2) (April 1998), 263–273.
[19] C.-L. Tsai, C.V. Stewart, H.L. Tanenbaum and B. Roysam, Modelbased method for improving the accuracy and repeatability of estimating vascular bifurcations and crossovers from retinal fundus images, *IEEE Trans Inf Technol Biomed* **8**(2) (June 2004), 122–130.
[20] K.A. Vermeer, F.M. Vos, H.G. Lemij and A.M. Vossepoel. A model based method for retinal blood vessel detection, *Comput Biol Med* **24** (2003), 209–219. 2003.
[21] L. Wang, A. Bhalerao and R. Wilson, Analysis of retinal vasculature using a multiresolution hermite model, *IEEE Trans Med Imag* **26**(2) (Feb. 2007), 137–152.
[22] D. Wu, M. Zhang and J.C. Liu, On the adaptive detection of blood vessels in retinal images. Technical report, Comput. Sci. Dept., Texas A&M Univ., College Station, March 2005.
[23] L. Zhou, M.S. Rzeszotarski, L.J. Singerman and J.M. Chokreff, The detection and quantification of retinopathy using digital angiograms, *IEEE Trans Med Imag* **13**(4) (Dec. 1994), 619–626.